separations

MDPI

Article

Research on the Flotation Mechanism of Microemulsion Collector Enhanced Removal of Dyeing Impurities from Phosphogypsum

Xiaosheng Yu [1], Lijun Deng [2], Changpan Shen [1], Huiyong Li [1,3], Jingchao Li [1], Yijun Cao [4,5], Guoli Zhou [1,4,*] and Guosheng Li [4,5,*]

[1] School of Chemical Engineering, Zhengzhou University, Zhengzhou 450001, China; 15093841721@163.com (X.Y.); 18339110935@163.com (C.S.); 18275287320@163.com (H.L.); chaoljc@163.com (J.L.)
[2] Center of Advanced Analysis & Gene Sequencing, Zhengzhou University, Zhengzhou 450001, China; okdenglijun@126.com
[3] Wengfu Group Co., Ltd., Guiyang 550002, China
[4] The Key Lab of Critical Metals Minerals Supernormal Enrichment and Extraction, Ministry of Education, Zhengzhou 450001, China; yijuncao@126.com
[5] Zhongyuan Critical Metals Laboratory, Zhengzhou University, Zhengzhou 450001, China
* Correspondence: zglcumt@126.com (G.Z.); lgscumt@163.com (G.L.); Tel.: +86-13-838-340-506 (G.Z.); +86-13-685-197-504 (G.L.)

Abstract: Phosphogypsum is an industrial byproduct that is limited in its high-value application due to the presence of dyeing impurities (such as organic matter and carbon black). The flotation method has been verified to be effective in separating these dyeing impurities from gypsum. In this study, microemulsion was used as the collector method of dyeing impurities for their separation from gypsum. The results of flotation tests showed that the microemulsion collector exhibited excellent collection capability and selectivity under natural pH conditions (pH = 1.5). With a microemulsion collector consumption of 400 g/t, purified gypsum of 65.1% whiteness, 95.74% yield, and 97.01% recovery was obtained. The purified gypsum of 65.1% whiteness, 95.74% yield, 97.01 recovery obtained by a used microemulsion collector amount of 400 g/t was better than using the same dosage of kerosene collector. The dispersion behavior of the microemulsion collector was studied by low-temperature transmission electron microscopy. The microemulsion collector demonstrated superior dispersibility, as it forms nano-oil droplets with an average size of 176.83 nm in the pulp, resolving issues associated with poor dispersibility observed in traditional kerosene collectors. Additionally, the nano-oil droplets effectively adsorbed onto the surface of dyeing impurities through hydrogen bonding, enhancing their hydrophobicity. Therefore, the microemulsion collector holds great potential for application in flotation whitening processes involving phosphogypsum.

Keywords: microemulsion; flotation; phosphogypsum; dyeing impurities

Academic Editor: Qicheng Feng

Received: 15 July 2024
Revised: 5 December 2024
Accepted: 11 December 2024
Published: 31 December 2024

Citation: Yu, X.; Deng, L.; Shen, C.; Li, H.; Li, J.; Cao, Y.; Zhou, G.; Li, G. Research on the Flotation Mechanism of Microemulsion Collector Enhanced Removal of Dyeing Impurities from Phosphogypsum. *Separations* **2025**, *12*, 7. https://doi.org/10.3390/separations12010007

1. Introduction

Phosphogypsum (PG) is an industrial by-product generated during the production of phosphoric acid from phosphate ore [1]. The main component of PG is $CaSO_4 \cdot 2H_2O$, with a content exceeding 85%, making it a valuable resource for gypsum regeneration [2]. According to statistics, for every ton of phosphoric acid produced, approximately 4 to 5 tons of PG are generated [3]. Due to the presence of dyeing impurities, mainly composed of carbon (including organic matter and carbon black), in PG, the whiteness of PG is low, and the color appears gray or gray black, severely limiting its high-value application in building

materials. As of now, the global cumulative production of PG has exceeded 7 billion tons [4], with only about 15% of PG being reused for construction materials, agricultural fertilizers, soil amendments, and Portland cement [5–8]. The extensive stacking of PG not only results in a significant waste of resources but also causes severe environmental pollution [9,10]. Therefore, the removal of impurities and whitening of PG are urgent and practical issues that need to be addressed.

The calcination method [11,12], acid leaching [13,14], and flotation [15,16] are commonly researched methods for whitening PG. However, both calcination and acid leaching methods suffer from high energy consumption, high costs, secondary pollution, and severe equipment corrosion, making industrial application challenging [17,18]. Flotation, as an efficient and environmentally friendly treatment method, has been widely used in many mineral separation tasks. Wang et al. [19] combined physical and chemical methods, first reacting PG with lime, and then using pine oil as a frother to remove dyeing impurities from the gypsum through reverse flotation. Finally, the whiteness of PG was increased from 31.3% to 58.4%. Du et al. [20] directly employed reverse flotation using methyl isobutyl carbinol (MIBC) as the frother to remove impurities from PG, resulting in a gypsum concentrate with a whiteness of 40.5%. Flotation reagents play a crucial role in flotation tests. Collectors also play a crucial role in flotation tests. However, the current research lacks an in-depth understanding of the dyeing impurities. Research has found that these impurities' surfaces contain abundant oxygen-containing functional groups (such as -OH and C=O), making them highly hydrophilic and poorly floatable. The simple use of pine oil and MIBC as frothers for reverse flotation makes it difficult to effectively separate dyeing impurities from gypsum, resulting in only a slight improvement in the whiteness of phosphogypsum concentrate. Therefore, for the purpose of whitening PG, the development of highly efficient flotation collectors is imperative.

The dyeing impurities mainly consist of carbonaceous material, for which traditional hydrocarbon oils (such as kerosene or diesel oil) can be used as collectors [21]. However, their poor dispersibility leads to inferior collection performance [22,23]. Numerous studies have indicated that preparing hydrocarbon oils into microemulsion collectors can yield favorable flotation results in mineral flotation tests [24]. Microemulsion collectors have not yet been applied in PG flotation but have been widely used in flotation processes for other minerals. For instance, Zhu et al. [25] optimized the formulation design of microemulsion collectors using a simplex lattice mixture design and pseudo-ternary phase diagrams. They prepared a microemulsion collector by compounding Gemini surfactants, diesel, n-octanol, and water, exhibiting excellent collecting capabilities. Qiao et al. [26] prepared a new type of oil-in-water microemulsion collector using DDA, kerosene, and water as the main components, and applied it to the flotation separation of quartz and magnetite. The microemulsion collector enhanced the hydrophobicity and floatability of quartz. The flotation performance was optimal when the microemulsion dosage was 45 g/t.

This study employed the Shah titration method to mix surfactants (fatty alcohol polyoxyethylene ether, AEO-9), a co-surfactant (n-butanol), an oil phase (kerosene), and water, preparing a non-ionic microemulsion to enhance the separation performance of PG. The superior collecting capability of the microemulsion collector was validated through flotation experiments. The dispersion behavior of the microemulsion in water was investigated using nano-laser particle size analysis and cryogenic transmission electron microscopy (Cryo-TEM). Additionally, the adsorption mechanism of the microemulsion collector on the surface of dyeing impurities was elucidated through contact angle measurements, Fourier-transform infrared spectroscopy (FT-IR), and X-ray photoelectron spectroscopy (XPS). The results of this study provide a new perspective for enhancing the purification and whitening of PG.

2. Experimental Section

2.1. Materials

The phosphogypsum (PG) used in this study was obtained from a large phosphorus chemical company in Longyan, Fujian, China. Wet sieving was employed to measure its particle size distribution, with −75 μm accounting for 52.36% and +75 μm for 47.64%. The whiteness of PG was determined using an intelligent whiteness meter, resulting in a value of 31.0%, with a purity of 88.65%. The X-ray fluorescence results of the PG samples in Table 1 indicate that PG mainly contains CaO and SO_3. Additionally, it contains small amounts of SiO_2, P_2O_5, MgO, Fe_2O_3, Al_2O_3, and BaO, among other components. Figures 1a and 1b respectively show the impurity distribution and carbon element analysis on the surface of PG crystals. The SEM image shows that there are numerous impurity particles attached to the gypsum crystals in the PG raw ore (Figure 1a). Through EDS surface scanning analysis, it is observed that the impurities contain a significant amount of carbon elements (Figure 1b). Additionally, the X-ray diffraction (XRD) pattern in Figure 2 indicated that the primary phases in the PG sample were dihydrate gypsum ($CaSO_4 \cdot 2H_2O$), with small amounts of calcium sulfate ($CaSO_4$) and quartz (SiO_2).

Table 1. X-ray fluorescence analysis of the PG sample (wt.%).

Components	CaO	SO_3	SiO_2	P_2O_5	MgO	Fe_2O_3	Al_2O_3	BaO
Content	31.41	39.07	4.16	1.69	0.21	0.19	0.14	0.02

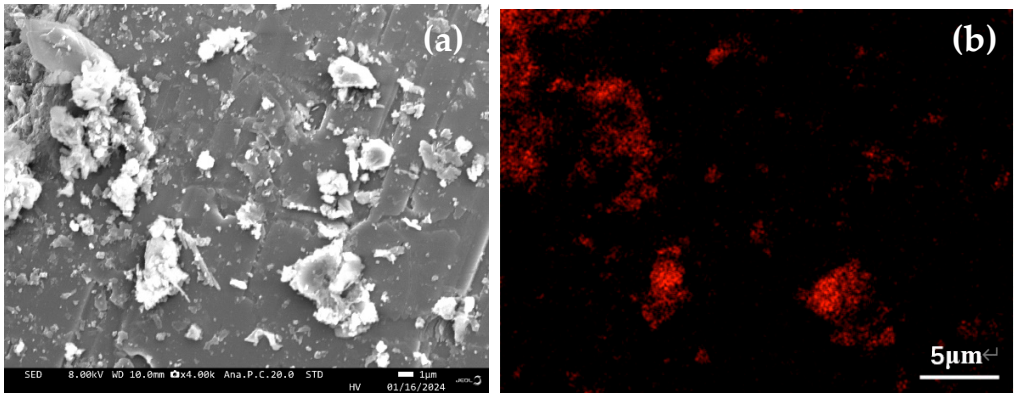

Figure 1. SEM images of PG sample ((**a**) the microstructure of and (**b**) the elements mapping scanning of the PG raw ore.)

The fatty alcohol polyoxyethylene ether (AEO-9) was purchased from Shanghai Yien Chemical Technology Co., Ltd. (Shanghai, China). As a green and efficient non-ionic surfactant, AEO-9 is an amphiphilic surfactant with a hydrophobic end consisting of a long-chain alkyl and a hydrophilic end formed by ring-opening polymerization of ethylene oxide. The molecular structure is R-O-$(CH_2CH_2O)_9$H, where R is a long-chain alkyl group composed of 12–18 carbon atoms. Compared to traditional ionic surfactants, AEO-9 has strong acid and alkali resistance, making it more suitable for the flotation of PG. Other chemicals such as n-butanol (purity 99.5%), kerosene (reagent grade), and methyl isobutyl carbinol (MIBC, purity 99%) were all purchased from Shanghai Yien Chemical Technology Co., LTD. (Shanghai, China). Microemulsion preparation used deionized water (18.2 MΩ·cm), and all flotation experiments used laboratory tap water. The gypsum (purity 98%) used for mechanism analysis was obtained from Zaozhuang Xianglin Gypsum Powder Co., Ltd., Zaozhuang, China, and the dyeing impurities were the previously mentioned separated and enriched dyeing impurities.

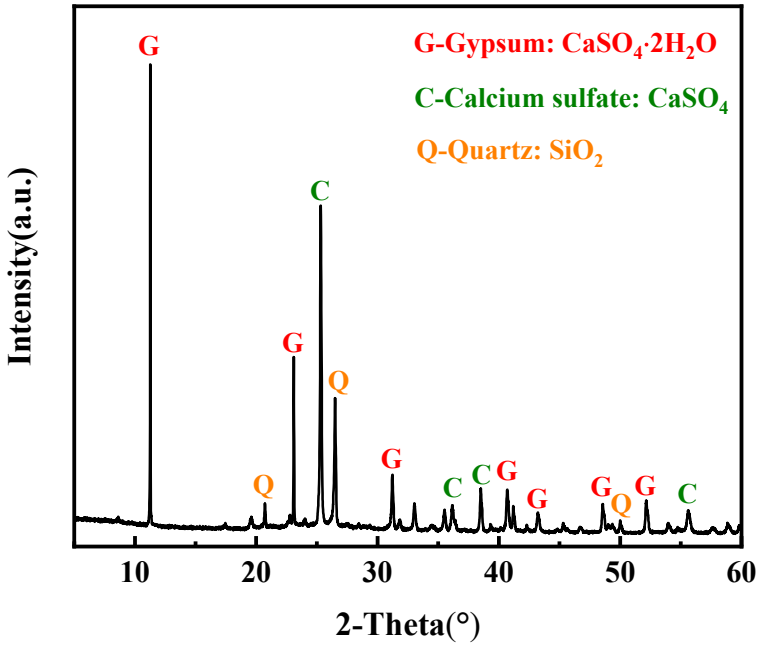

Figure 2. XRD pattern of the PG sample.

2.2. Methods

2.2.1. Preparation of Microemulsion and Its Dispersion Process

The microemulsion collector was prepared with a composite of AEO-9, n-butanol, kerosene, and water in mass ratios of 14.69%, 14.69%, 59.32%, and 11.30%, respectively, according to the steps shown in Figure 3a. Initially, the surfactant and co-surfactant were mixed in proportion to form an emulsifier, named SAX. Subsequently, kerosene and deionized water were separately added to the emulsifier. The mixture was stirred using a magnetic stirrer at room temperature, with stirring speed and duration set at 500 r/min and 5 min, respectively.

To investigate the dispersion behavior of the microemulsion collector, the microemulsion was introduced into 0.75 L of water to simulate its dispersion process in pulp. Mechanical stirring at 1800 r/min for 3 min was employed to study its dispersion behavior. As a control, the dispersion behavior of the kerosene collector in the mineral slurry was investigated under identical conditions to the microemulsion collector.

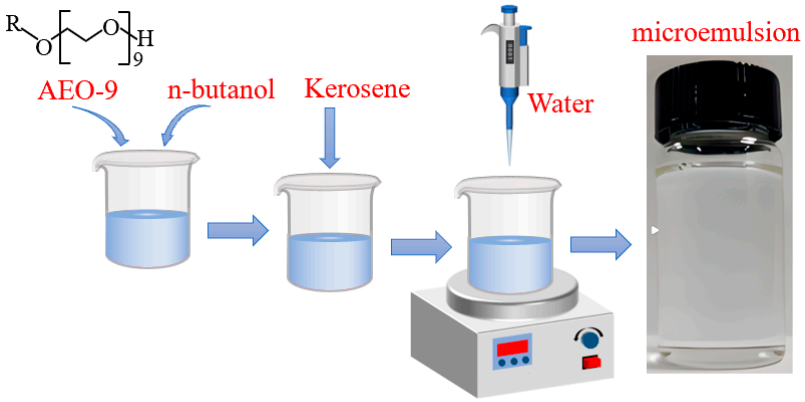

(a) Flow chart of microemulsion preparation

Figure 3. *Cont.*

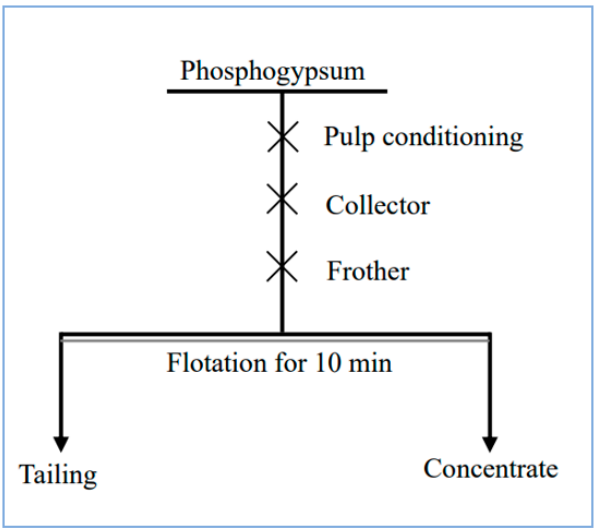

(b) Flow chart of the flotation tests

Figure 3. Flow chart of microemulsion preparation (**a**) and the reverse flotation tests (**b**).

2.2.2. Flotation Tests

To compare the flotation capabilities of the microemulsion collector and kerosene, reverse flotation tests was conducted on PG using a 0.75 L single-slot flotation machine (XFD, Wuhan Exploring Machinery Co., Ltd., Wuhan, China). The pulp concentration was 30%. The flow chart for the flotation tests is shown in Figure 3b. First, the pulp was stirred at an impeller speed of 1800 r/min for 3 min in the flotation cell, and the collector was subsequently added. After 3 min, the frother was added and inflated for 30 s (airflow rate of 0.18 m^3/h). Subsequently, a 10 min scraping operation was carried out. After completing the flotation test, the concentrate and tailings were dried, weighed, and measured for whiteness and purity. When using kerosene as the collector, the frother employed was methyl isobutyl carbinol (MIBC). For the microemulsion collector, no additional frother was needed due to its inherent foaming properties.

2.2.3. Whiteness Detection

The sample's whiteness was determined using an intelligent whiteness measurement instrument (WSB-X, Hangzhou Dacheng Optoelectronic Instrument Co., Ltd., Hangzhou, China). Initially, the sample was compressed into a tablet, and subsequently placed on the detection platform. After each measurement, the sample was rotated by 90° for the next measurement, and this process was repeated four times to obtain an average value.

2.2.4. Purity Testing

The content of $CaSO_4 \cdot 2H_2O$ in PG was calculated according to the formula [16,27],:

$$G = 4.7785 \times H \quad (1)$$

where G is the mass fraction of calcium sulphate dihydrate (%), 4.7785 is the molecular weight of calcium sulphate dihydrate divided by the molecular weight of two water molecules, which is the conversion coefficient of calcium sulphate dihydrate content from the crystal water content. H is the content of crystal water (%), which was determined according to the drying-loss method [16,27].

2.2.5. Droplet Size Measurements

The droplet size was measured using a nano-laser particle size analyzer (Nano ZSE, Malvern, UK). Using a syringe, 1 mL of the prepared sample was injected into a cuvette for measurement. Each sample was measured three times at 25 °C, and the average value was recorded.

2.2.6. Cryogenic-Transmission Electron Microscopy Characterizations

A Cryo-TEM (Glacios, Thermo Scientific, Waltham, MA, USA) was used to study the microscopic morphology of the microemulsion droplets. First, 3 μL of the sample was pipetted onto a copper grid for sample preparation. The sample was rapidly frozen in liquid nitrogen and then transferred to the Cryo-TEM for observation.

2.2.7. Contact Angle Measurements

The contact angle measurements were conducted using an optical contact angle tester (Theta Flex, Biolin, Gothenburg, Finland). Prior to the contact angle measurement, the dyeing impurities and gypsum before and after treatment with the collector were ground into fine particles. The dyeing impurities or gypsum sample (1.0 g) were pressed into a dense sheet with a thickness of approximately 2 mm using a tablet press at 20 MPa for 15 min. Deionized water droplets were added to the surface of the sample, and the contact angles were recorded.

2.2.8. Fourier Transform Infrared Spectroscopy (FT-IR) Measurements

Fourier transform infrared spectroscopy (Nicolet iS20, Thermo Scientific, Waltham, MA, USA) was used to analyze the functional groups on the surface of the dyeing impurities and gypsum before and after treatment with the collector. First, 100 mg KBr was mixed with 1 mg of dyeing impurities or gypsum, ground, and pressed into a transparent sheet. The instrument has a scanning range of 4000–400 cm^{-1} and a spectral resolution of 4 cm^{-1}.

2.2.9. X-Ray Photoelectron Spectroscopy (XPS) Measurements

XPS (K-Alpha, Thermo Scientific, USA) was used to characterize the staining impurities before and after collector treatment, mainly to detect changes in the content of hydrophobic and hydrophilic functional group on the surface of the staining impurities. The XPS peak 4.1 software was used to further peak fit the narrow scan spectra of the colored impurity samples and calculate the relative content of each functional group on the surface of the colored impurities. The narrow scan binding energy data of each element was calibrated using the C1s peak (284.8 eV) as a reference.

3. Results and Discussion

3.1. Analysis of Dyeing Impurities

This study employed a water-washing method to separate and enrich the coloring impurities from the original PG ore. The enriched dyeing impurities underwent thermogravimetric analysis (TG), total organic carbon analysis (TOC), and elemental analysis (EA). Through thermogravimetric analysis, a weight loss of 9.96% between 106 and 143 °C was attributed to the loss of the crystallization water of the calcium sulphate dihydrate. Furthermore, in the temperature range of 143–571 °C, the sample lost 20.11% of its weight, primarily due to the decomposition of carbonaceous matter in the sample (Figure 4). According to the results from Table 2, the total carbon content in the dyeing impurities was determined to be 21.66%, aligning with the thermogravimetric analysis findings. As indicated in Table 2 for elemental analysis of the dyeing impurities, the organic carbon content stood at 10.82%, which corresponded to the 11.21% organic carbon content determined through total organic

carbon analysis. In addition, the oxygen content was as high as 20.51%, indicating that the dyeing impurities may contain a large amount of oxygen-containing functional groups.

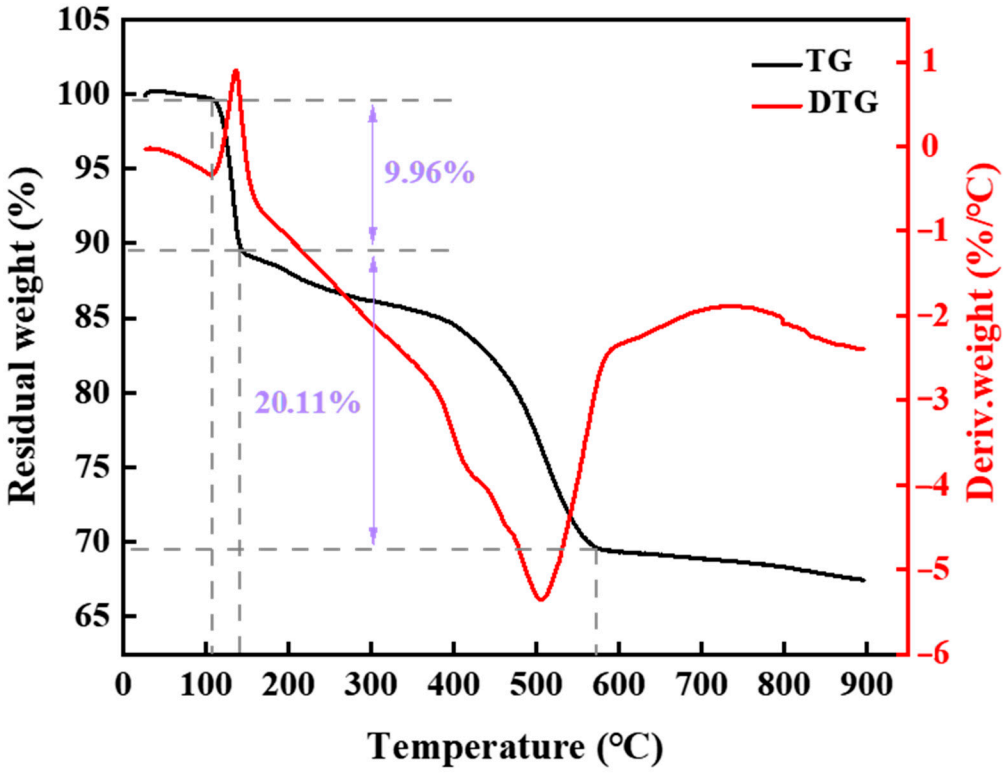

Figure 4. TG-DTG pattern of the dyeing impurities.

Table 2. Total organic carbon and organic elements analysis of dyeing impurities (wt.%).

Index	Total Organic Carbon Analysis		Organic Element Analysis				
	TC	TOC	C	H	O	N	S
Result	21.66	11.21	10.82	1.85	26.50	0.32	15.55

3.2. Dispersion Behavior of the Microemulsion and Kerosene

When preparing the microemulsion system of AEO-9/n-butanol/kerosene/water, the droplet size distribution of the microemulsion was determined, as shown in Figure 5a. The droplet size distribution of the microemulsion was within the range of 20–100 nm, with an average particle size of 23.15 nm, indicating that the mixed system conforms to the definition of a microemulsion (10–100 nm).

In the flotation process, hydrocarbon oil collector is added to the ore pulp and dispersed into oil droplets. Many scholars have already proven that the smaller the size of the oil droplets, the higher the probability of their collision with mineral particles, making it easier for the collector to adsorb onto the surface of mineral particles. Common non-polar hydrocarbon collectors, due to their natural hydrophobic nature, exhibit poor dispersibility in water and often exist in the pulp in the form of large oil droplets (>0.1 mm), leading to poor flotation outcomes [28]. Microemulsions, as thermodynamically stable systems with particle sizes ranging between 10 and 100 nm, demonstrate good dispersibility in water due to the presence of surfactants and co-surfactants. Research indicates that the droplet sizes of microemulsions dispersed in water are much smaller than those of traditional non-polar hydrocarbon oils dispersed in water [29], providing a possibility for their use as flotation collectors. To verify this conclusion, we dispersed microemulsions and kerosene separately

in water, simulating their dispersibility in the pulp, and the size distribution and of the oil droplets generated by their dispersion were measured.

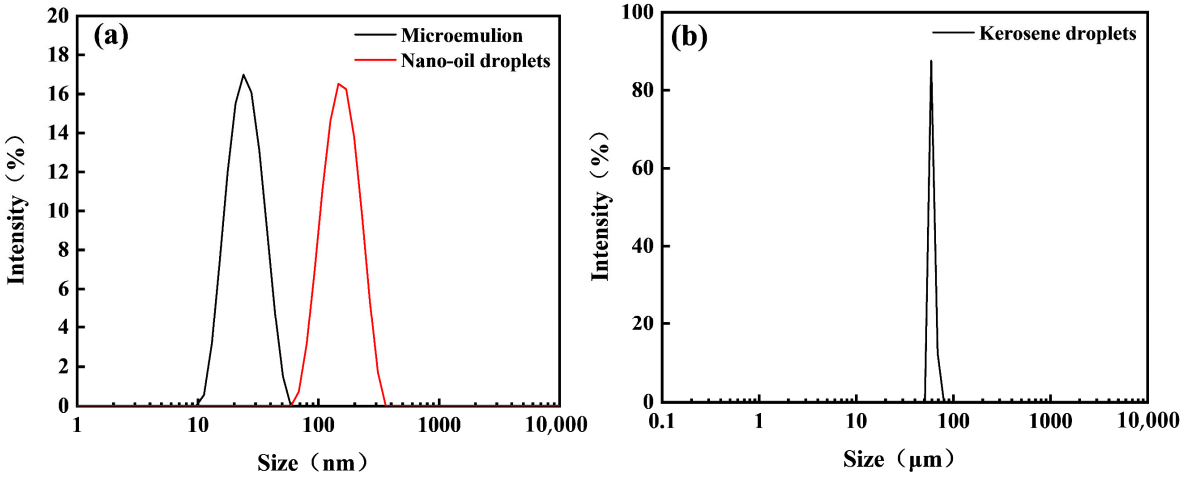

Figure 5. Size distribution of oil droplets generated by the dispersion of the microemulsion (**a**) and kerosene (**b**).

The particle size distribution of oil droplets generated by the dispersion of microemulsion and kerosene is illustrated in Figure 5. As shown in the Figure 5a, the size distribution of oil droplets produced by microemulsion dispersion falls within the range of 60–300 nm, with an average particle size of 176.83 nm. This indicates that microemulsions can disperse into nanoscale oil droplets in water. From Figure 5b, it can be observed that the size of oil droplets generated by the dispersion of kerosene in water is much larger than that of microemulsion dispersion. The droplet size distribution ranges between 50 and 110 μm, with an average size of 70.23 μm. The oil droplets generated by the dispersion of kerosene were larger in size, making it difficult for them to collide with dyeing impurities and be adsorbed on the surface of dyeing impurities, which is detrimental to the flotation of phosphogypsum.

Using cryo-transmission electron microscopy, we further investigated the micromorphology and dispersion behavior of microemulsions from a microscopic perspective. The micromorphology of the microemulsion is shown in Figure 6a. The microemulsion employed in this study is a complex dispersed system composed of a continuous oil phase, water cores, and oil–water interfaces. The water cores were surrounded by an oil–water interface consisting of surfactants and cosurfactants. The particle sizes of the microemulsion vary but are all less than 100 nm. The micromorphology of the microemulsion is approximately spherical, and it exists in a dispersed state. The average size of the microemulsion is estimated to be around 25 nm according to the scale, consistent with the size measured by the nano-laser particle size analyzer. In Figure 6b, it is indicated that the microemulsion disperses into nanoscale oil droplets with a particle size of approximately 180 nm. Upon introducing the microemulsion into water, some of the surfactants and co-surfactants will diffuse into the water, leading to the disruption of thermodynamic stability [30]. Mechanical stirring accelerates the migration of surfactants and co-surfactants, promoting the formation of new oil–water interfaces and resulting in the formation of nanoscale oil droplets. After the generation of new oil–water interfaces, the hydrophobic alkyl chains of the non-ionic surfactant (AEO-9) enter the oil phase, while the hydrophilic ether bonds are exposed in the aqueous phase.

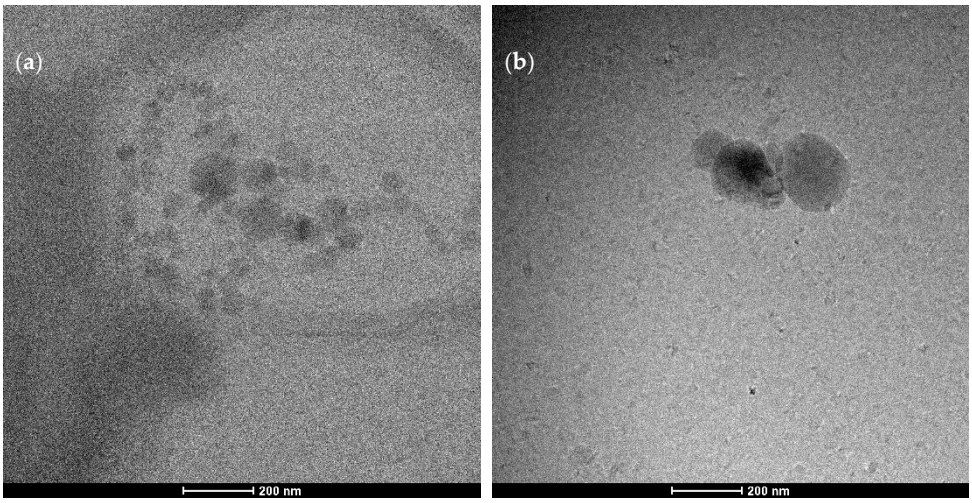

Figure 6. Morphology of the microemulsion (**a**) and nano-oil droplets (**b**).

3.3. Analysis of Test Results of Flotation Purification

To explore the influence of collector dosage on the flotation performance of PG, the kerosene and the microemulsion collectors were used in the flotation tests. All flotation tests were performed under a natural pH (pH = 1.5) condition, and the flotation test results are shown in Figure 7.

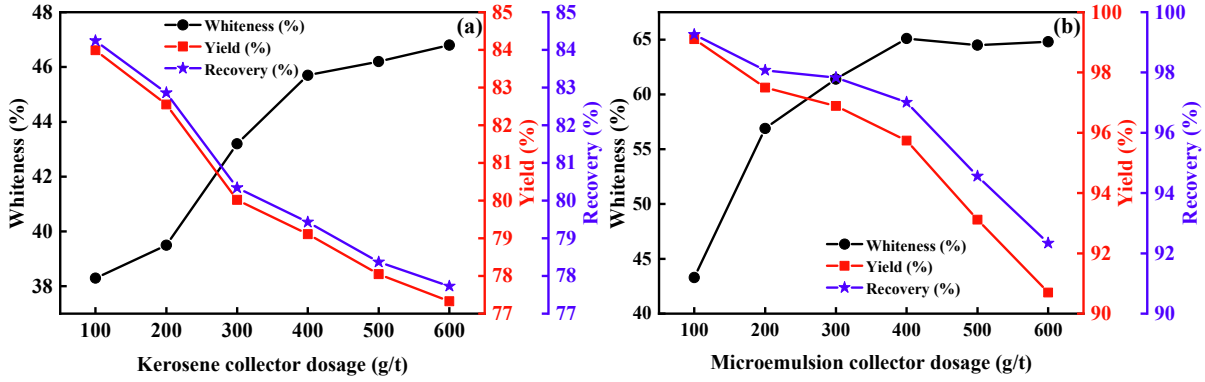

Figure 7. Flotation results at different dosages of kerosene (**a**) and microemulsion (**b**) collectors.

Figure 7a indicates that the kerosene collector has a relatively poorer flotation performance in terms of improving the whiteness of PG, with only a slight improvement in the whiteness of the flotation gypsum concentrate compared to the original PG. As the kerosene dosage increased, the whiteness index of the concentrate first increases significantly and then stabilizes, while the yield and recovery rate continue to decrease. When the kerosene dosage reached 400 g/t, appropriate flotation performance was achieved, with whiteness, yield, and recovery rates of 45.7%, 79.11%, and 79.43%, respectively. Figure 7b demonstrates the influence of microemulsion collector dosage on the flotation performance of PG. As the consumption of microemulsion collector increases, the trend of flotation indices is similar to that of the kerosene. Compared to traditional kerosene, the microemulsion collector exhibits higher flotation efficiency. With a microemulsion collector consumption of 400 g/t, purified gypsum with a concentrate whiteness, yield, and recovery rate of 65.1%, 95.74%, and 97.01% was obtained.

From the flotation results, when both the kerosene collector and microemulsion collector are at their optimal dosages, the flotation performance of the microemulsion collector compared to kerosene shows an increase in concentrate whiteness, yield, and recovery rate by 19.4%, 16.63%, and 17.58%, respectively, indicating that the microemulsion collector

possesses relatively better flotation performance. When using kerosene as the collector, severe foam entrainment leads to lower yield and recovery. In contrast, the microemulsion collector exhibits superior selectivity, maintaining higher levels of yield and recovery. However, when the dosage of the microemulsion collector increases from 400 g/t to 600 g/t, both the yield and recovery rates significantly decrease.

It when the dosage reaches a certain level, the selectivity of the microemulsion collector diminishes. This phenomenon arises from the non-selective adsorption between the microemulsion collector and gypsum due to the presence of a surfactant (AEO-9 in this study). Upon excessive addition of the microemulsion collector to the pulp, not only do ether bonds of fatty alcohol polyoxyethylene ether adsorb onto the dyeing impurities' surfaces but also onto the surface of the gypsum, resulting in a significant amount of gypsum entering the tailings, and consequently leading to lower concentrate yield and recovery. Furthermore, an increase in microemulsion collector dosage exacerbates foam entrainment, causing a decline in concentrate yield and recovery. Therefore, it is advisable to conduct actual flotation processes at relatively lower dosages of the microemulsion collector for improved flotation performance.

The microscopic morphologies of original PG and gypsum concentrate were observed by SEM, and the results are shown in Figure 8. As shown in Figure 8a, the surface of the original PG crystal adsorbs a large amount of staining impurities. The gypsum concentrate obtained through reverse flotation using a microemulsion collector is shown in Figure 8b. The surface of gypsum crystals in the gypsum concentrate is smoother and cleaner, and a large amount of dyeing impurities are effectively removed, which is the main reason for the significant improvement in the whiteness of the obtained PG. At this time, the purity of the gypsum concentrate is 95.81%, which reaches the first-grade national standard of PG in China (GB/T 23456-2018) and can be directly used to produce building materials such as gypsum boards and gypsum powder.

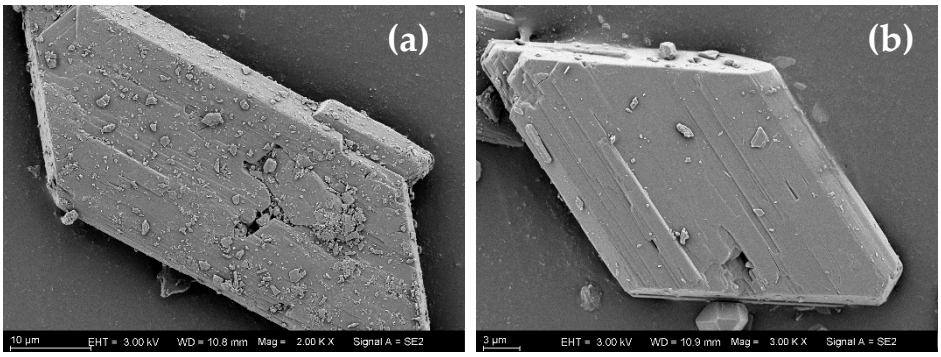

Figure 8. SEM images of raw PG (**a**) and gypsum concentrate (**b**).

3.4. Mechanism Analysis

3.4.1. Contact Angle Measurement Results

The contact angle can be used to evaluate the hydrophobicity and floatability of minerals from a macroscopic perspective [31]. In order to investigate the adsorption effects of kerosene and microemulsion collector on the surfaces of dyeing impurities and gypsum, the contact angles of gypsum and dyeing impurities before and after treatment with the kerosene and microemulsion collectors (both collector dosages are set at 2 kg/t and treatment time at 3 min) were measured, and the results are shown in Figure 9.

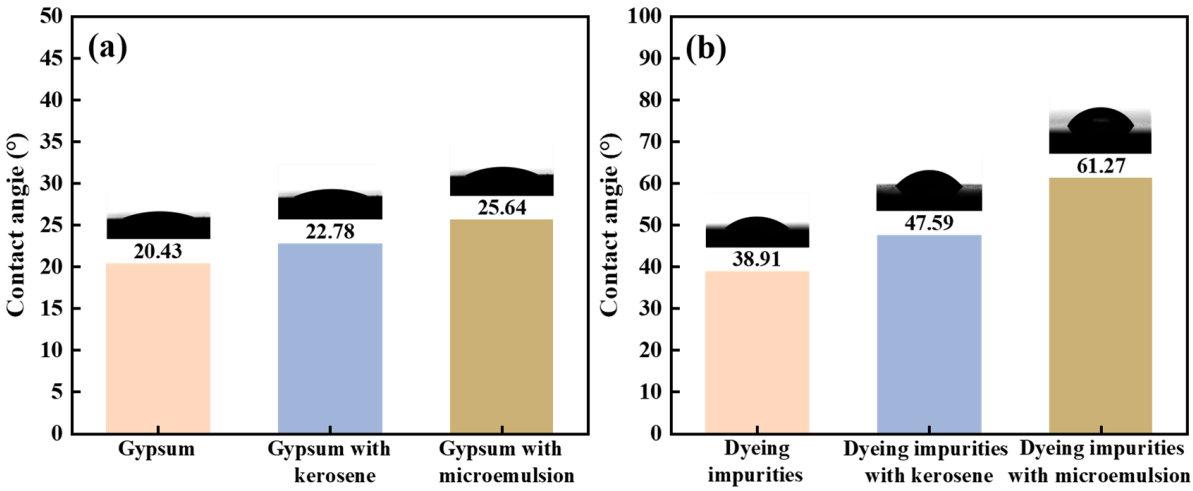

Figure 9. Contact angles of gypsum (**a**) and dyeing impurities (**b**) before and after being treated with kerosene and microemulsion.

The contact angle of gypsum is 20.43°, as shown in Figure 9a. Following treatment with kerosene and microemulsion collectors, the contact angle slightly increases to 22.78° and 25.64°, respectively, indicating minimal impact on the hydrophobicity and floatability of gypsum by these collectors. As shown in Figure 9b, the contact angle of dyeing impurities is 38.91°, suggesting their poor hydrophobicity due to an abundance of oxygen-containing functional groups on the surface. However, when the kerosene is employed as a collector, it slightly enhances the hydrophobicity of the dyeing impurities' surfaces, as evidence by an increased contact angle of 47.59°. This improvement is limited due to the poor dispersibility of kerosene in the pulp, which hinders its dispersion and adsorption onto the impurity surface, resulting in a limited improvement in the flotation performance of the dyeing impurities. In contrast to kerosene, the microemulsion collector exhibits excellent dispersibility in the pulp, which can be dispersed into nano-oil droplets. Simultaneously, the ether bonds in the fatty alcohol polyoxyethylene ether combine with the oxygen-containing functional groups on the surface of dyeing impurities through hydrogen bonding. This interaction provides more hydrophobic sites on the surface of dyeing impurities, enabling the nano-oil droplets to more effectively adsorb onto the surface of the dyeing impurities. After treatment with the microemulsion collector, the contact angle increased to 61.27°, indicating that the microemulsion collector can more effectively enhance the surface hydrophobicity and floatability of the dyeing impurities [32].

3.4.2. Fourier Transform Infrared Spectroscopy (FT-IR) Analysis

FT-IR is an important method for analyzing the functional groups on the surface of dyeing impurities. The FT-IR results for the collectors, gypsum, and dyeing impurities before and after treatment with kerosene and microemulsion collectors (the dosage of both collectors is 2 kg/t and the treatment time is 3 min) are shown in Figure 10. The FT-IR results for the kerosene and microemulsion collectors are shown in Figure 10a. The absorption peaks at 2955 and 2921 cm^{-1} correspond to the asymmetric stretching vibrations of aliphatic hydrocarbon -CH_3 and -CH_2, while the peaks at 2871 and 2853 cm^{-1} represent the symmetric stretching vibrations of aliphatic hydrocarbon -CH_3 and -CH_2. The absorption peaks at 1460 and 1377 cm^{-1} correspond to the deformation vibrations of -CH_2 and -CH_3 attached to N and O atoms, respectively [33]. The peak at 3382 cm^{-1} corresponds to the vibrational absorption of -OH in water, while the peaks at 1112 and 949 cm^{-1} correspond to the asymmetric and symmetric stretching vibrations of C-O-C in AEO-9, respectively [34].

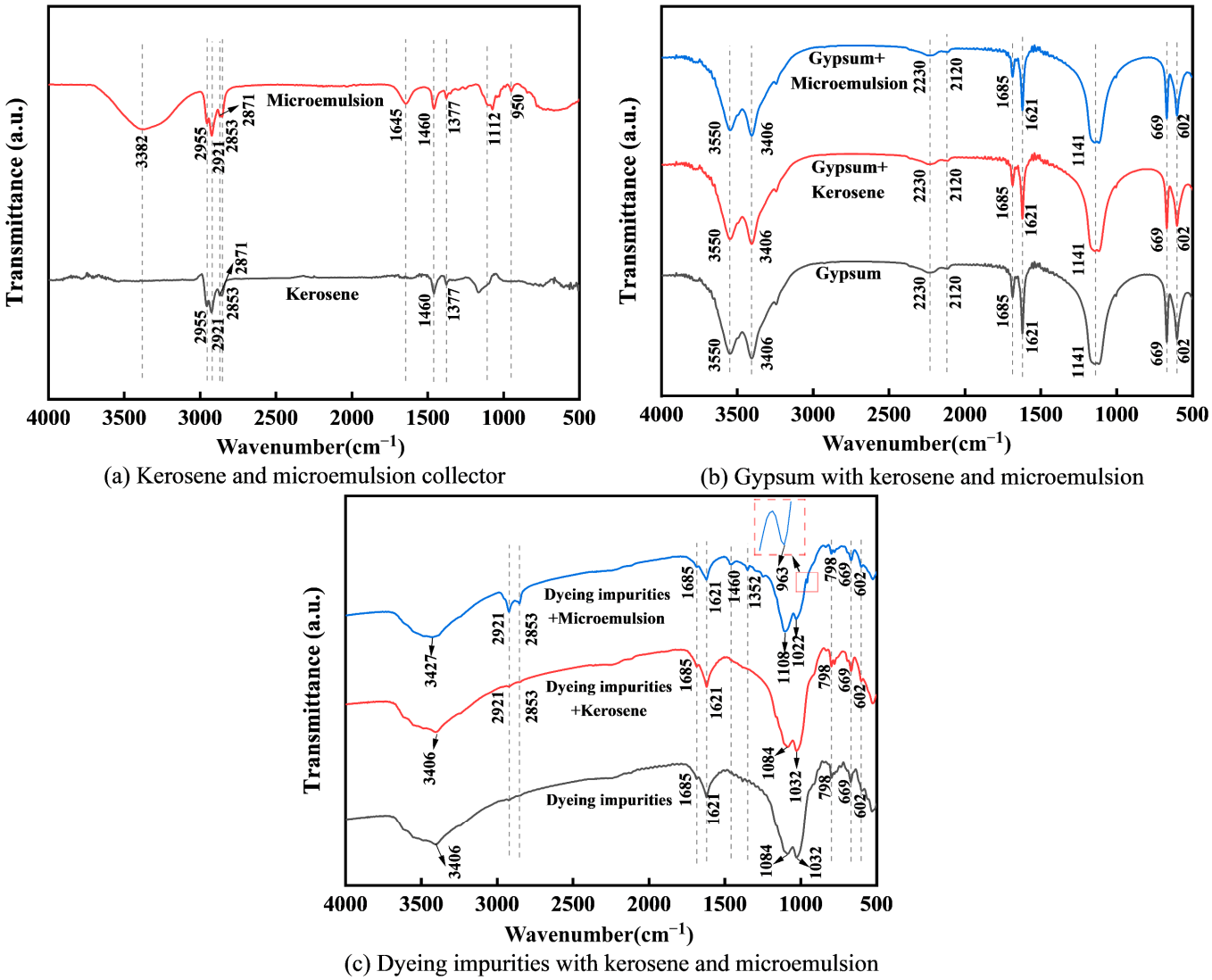

Figure 10. FT-IR results of gypsum and dyeing impurities treated by different collectors.

The FT-IR results of gypsum before and after treatment with kerosene and microemulsion collector are presented in Figure 10b. The peaks at 3550 and 3406 cm^{-1} correspond the stretching vibrations of -OH groups, while the peaks at 1685 and 1621 cm^{-1} are attributed to the typical bending vibrations of crystalline water in gypsum. Additionally, the characteristic peaks appearing at 1141 cm^{-1}, 669 cm^{-1}, and 602 cm^{-1} are attributed to the stretching and bending vibrations of S=O and S-O bonds [35]. Compared to the FT-IR spectrum of gypsum, no new peaks or peak shifts were detected in samples treated with kerosene or microemulsion collectors. This indicates that these agents have minimal adsorption onto the surface of gypsum. Although it is theoretically possible for hydrogen bonding interactions between microemulsion collectors and gypsum particles to exist within this system, the FT-IR results demonstrate that the interaction is very weak.

The FT-IR results of dyeing impurities before and after treatment with kerosene and microemulsion collector are shown in Figure 10c. From the figure, it can be observed that the peaks at 798 and 1084 cm^{-1} are due to the symmetric and asymmetric vibrations of Si-O in quartz, indicating the presence of SiO_2 [36]. The peak at 1032 cm^{-1} corresponds to the C-O stretching vibration peak, which is an important component of the oxygen-containing functional group on the surface of dyeing impurities. There is no obvious difference in the basic characteristic peaks of the dyeing impurities treated by the two collectors, indicating

that the physical adsorption of both collectors dominates the flotation of the dyeing impurities. After treatment by the kerosene collector, the aliphatic -CH_2 vibration peak of the kerosene is detected in the FT-IR spectrum of the dyeing impurities at 2921 and 2853 cm^{-1}, indicating that the kerosene can be adsorbed on the surface of the dyeing impurities. In contrast, after the dyeing impurities are treated with the microemulsion collector, the peak intensities at 2921 and 2853 cm^{-1} significantly increased. Additionally, new absorption peaks corresponding to the deformation vibrations of -CH_2 and -CH_3 appeared at 1460 and 1352 cm^{-1}, indicating that the microemulsion collector can be adsorbed on the surface of the dyeing impurities more effectively. At the same time, it can be observed that the characteristic peak of -OH at 3406 cm^{-1} has shifted to 3427 cm^{-1}; the intensity of the characteristic peak of C-O at 1103 cm^{-1} has significantly weakened and shifted to 1022 cm^{-1}; and the characteristic peak of C-O-C in AEO-9 has shifted from 950 cm^{-1} to 963 cm^{-1}. The shifts in the above peaks indicate that the microemulsion collector has formed hydrogen bonds with the oxygen-containing functional groups on the surface of the dyeing impurities.

3.4.3. X-Ray Photoelectron Spectroscopy (XPS) Analysis

XPS is used to further study the influence of the kerosene and microemulsion collectors on the hydrophobic and hydrophilic functional groups of the dyeing impurities [37]. The fitting results of the C 1s energy spectrum of original dyeing impurities and the dyeing impurities treated with the kerosene and microemulsion collectors (the dosage of both collectors is 2 kg/t and the treatment time is 3 min) are shown in Figure 11. The binding energy positions at 284.8, 286.3, and 287.5 eV correspond to C-C/C-H, C-O, and C=O, respectively [38]. The relative content of each functional group was calculated based on the peak area. The fitting results of the original dyeing impurities are shown in Figure 11a, with relative contents of C-C/C-H, C-O, and C=O at 55.25%, 32.6%, and 12.15%, respectively. The presence of oxygen-containing functional groups increases the surface hydrophilicity of the dyeing impurities, leading to poor flotation performance.

The hydrophobic collector enhances its hydrophobicity by adsorbing onto the dyeing impurities, and the adsorption effectiveness is evaluated based on the relative content of oxygen functional groups on the surface of the dyeing impurities. As shown in Figure 11b, after treating the dyeing impurities with the kerosene collector for hydrophobic modification, the hydrophobic C-C/C-H content on the surface of the dyeing impurities increased to 61.29%, while the contents of the hydrophilic C-O and C=O decreased to 29.12% and 9.59%, respectively. As shown in Figure 11c, when using the microemulsion collector, the C-C/C-H content on the surface of the dyeing impurities significantly increased to 74.52%, while the C-O and C=O contents decreased to 19.69% and 5.79%, respectively. The XPS results indicate that the floatability was significantly improved after hydrophobic modification of the dyeing impurities using the microemulsion collector.

Furthermore, after kerosene treatment, the binding energy positions of C-O and C=O in the dyeing impurities remained unchanged compared to the original dyeing impurities. However, after treatment by the microemulsion collector, the binding energy positions of C-O and C=O shifted from 286.3 eV and 287.5 eV to 286.7 eV and 288.1 eV, respectively. It is speculated that this shift is due to the hydrogen bonding interaction between the microemulsion collector and the oxygen-containing functional groups on the surface of the dyeing impurities.

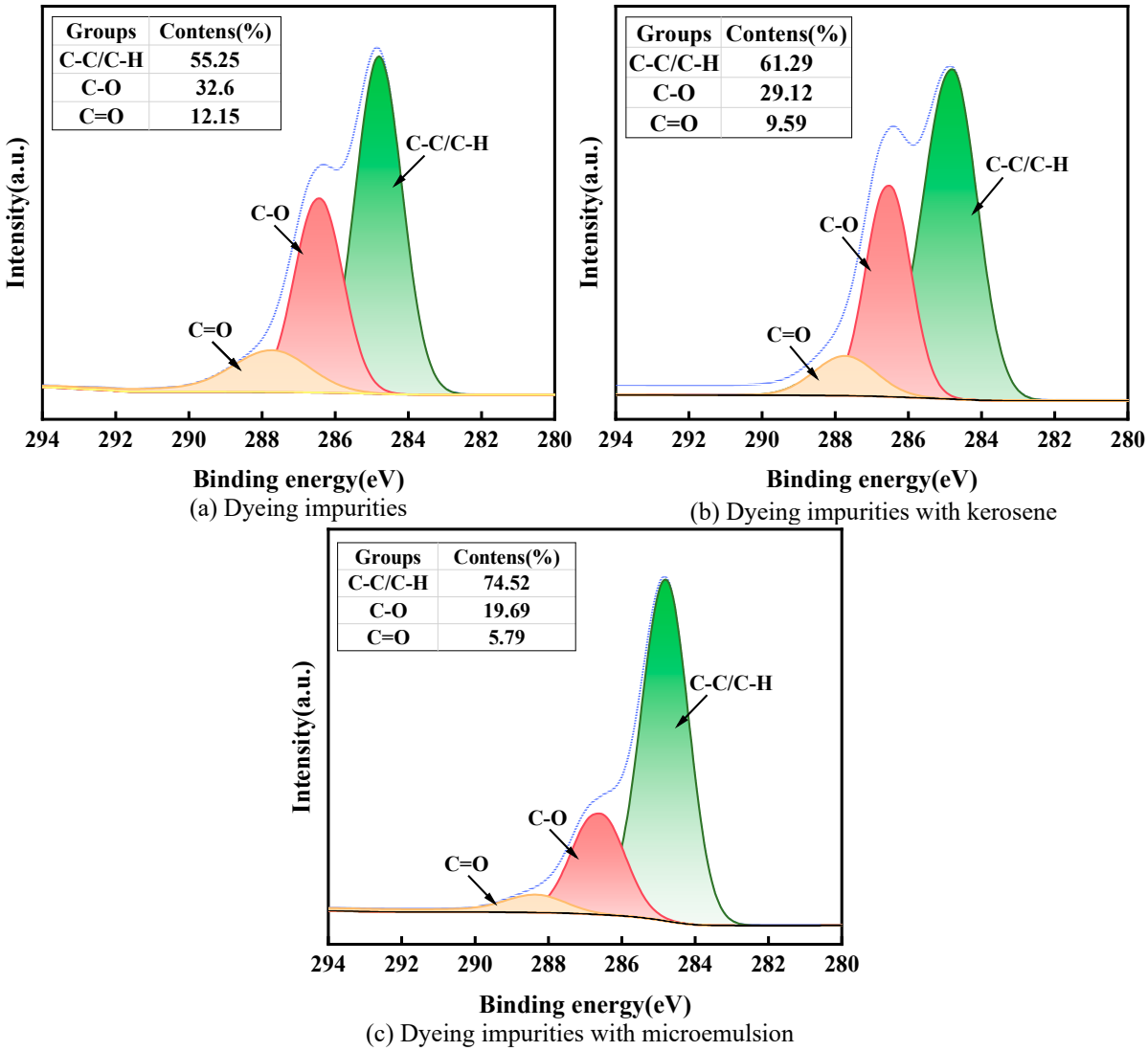

Figure 11. XPS results of dyeing impurities treated by different collectors.

Based on the above mechanistic analysis, it can be concluded that the use of microemulsion as a collector significantly improves the flotation performance of dyeing impurities. This is mainly due to the nano-oil droplets produced after the dispersion of the microemulsion, which significantly enhances the dispersibility of traditional collectors. In addition, the fatty alcohol polyoxyethylene ether (AEO-9) in the microemulsion collector forms hydrogen bonds with the oxygen-containing functional groups (-OH, C-O, C=O) on the surface of the dyeing impurities, effectively adsorbing in the hydrophilic regions of the dyeing impurities. After spreading on the surface of the dyeing impurities, the nano-oil droplets cover the oxygen-containing functional groups on the dyeing impurities' surface, significantly increasing the hydrophobicity of the dyeing impurities. A schematic diagram illustrating the improvement in the flotation performance of PG by the microemulsion collector is shown in Figure 12.

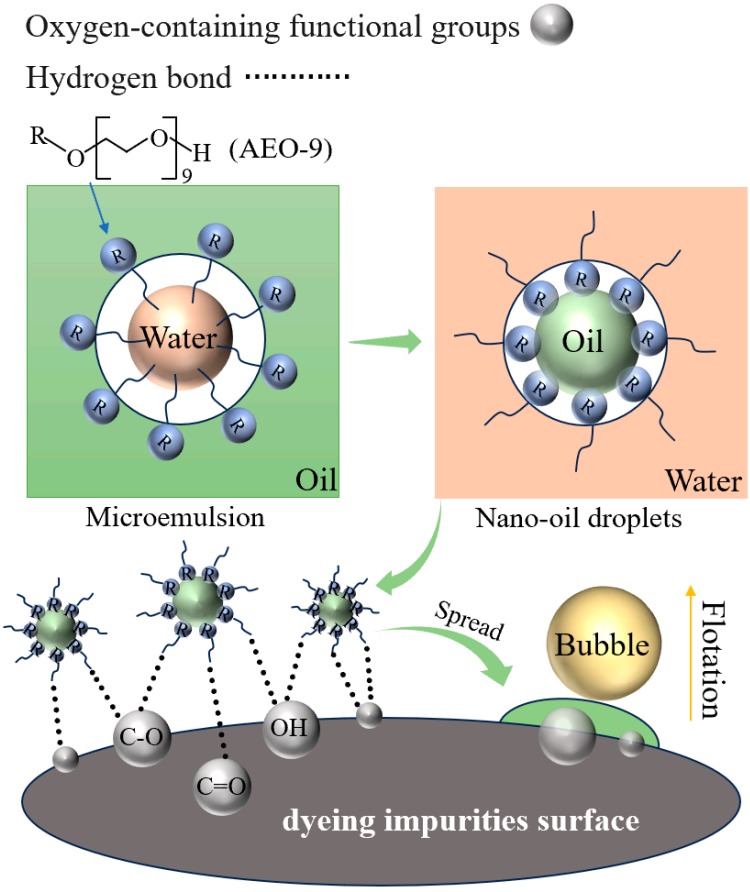

Figure 12. Schematic diagram of the microemulsion collector enhancing flotation performance of PG.

4. Conclusions

The microemulsion collector was first used in the flotation separation of dyeing impurities from gypsum, which exhibits superior capturing capability and selectivity for natural pH conditions. Based on the obtained results, the interaction mechanism of the microemulsion collector in enhancing the flotation performance of phosphogypsum (PG) was investigated. The following results were obtained:

(1) The dyeing impurities have a large number of oxygen-containing functional groups on their surfaces, which makes them highly hydrophilic and weakly hydrophobic.

(2) The microemulsion collector exhibited excellent dispersibility in water and could form oil droplets with an average size of 176.83 nm. Cryo-TEM revealed that the thermodynamic stability of the microemulsion was disrupted under mechanical agitation, leading to the formation of new nano-oil droplets.

(3) Satisfactory flotation indices could be obtained by using the microemulsion collector at a dosage of 6 kg/t. Compared to an equal dosage of kerosene collector, the whiteness, yield, and recovery rate of the concentrate improved by 19.4%, 16.63%, and 17.58%, respectively. The highly efficient flotation performance of the microemulsion collector can be attributed to the high collision probability and hydrogen bond attraction between the microemulsion collector and the dyeing impurities.

(4) The contact angle measurement indicated that the microemulsion collector is more easily adsorbed onto the surface of the dyeing impurities, resulting in the hydrophobicity of the dyeing impurities being significantly improved. FT-IR and XPS analyses indicated that hydrogen bond attraction was the driving force for adsorption. After adsorption of the microemulsion collector, the oxygen-containing functional groups on the surface of the dyeing

impurities are covered. The relative content of surface oxygen-containing functional groups (C-O, C=O) decreases significantly, while the content of C-C/C-H increases significantly.

Author Contributions: Conceptualization, H.L. and J.L.; methodology, X.Y. and L.D.; validation, C.S.; date curation, X.Y. and C.S.; formal analysis, H.L.; writing—original draft, X.Y.; writing—review and editing, L.D. and G.Z.; supervision, Y.C. and G.Z.; project administration, G.L.; funding acquisition, G.Z. and G.L. All authors have read and agreed to the published version of the manuscript.

Funding: This work was financially supported by the National Science Foundation of China (No. 52374281, No. 52204287) and the Innovative Research Team (in Science and Technology) at the University of Henan Province (19IRTSTHN028).

Data Availability Statement: Data are contained within the article.

Conflicts of Interest: Author Huiyong Li was employed by the company Wengfu Group Co., Ltd. The remaining authors declare that the research was conducted in the absence of any commercial or financial relationships that could be construed as a potential conflict of interest.

References

1. Eliwa, A.A.; Mubark, A.E.; Abdelfattah, N.A.; El Gawad, E.A. Maximizing the exploitation of phosphogypsum wastes using soaking technique with citric acid, recovering rare-earth and residual phosphate contents. *J. Cent. South Univ.* **2022**, *29*, 3896–3911. [CrossRef]
2. Pliaka, M.; Gaidajis, G. Potential uses of phosphogypsum: A review. *J. Environ. Sci. Health Part A* **2022**, *57*, 746–763. [CrossRef] [PubMed]
3. Zeng, C.; Guan, Q.; Sui, Y.; Yu, W.; Bu, Y.; Liu, C.; Zhang, Z. Kinetics of nitric acid leaching of low-grade rare earth elements from phosphogypsum. *J. Cent. South Univ.* **2022**, *29*, 1869–1880. [CrossRef]
4. Mashifana, T. Chemical treatment of phosphogypsum and its potential application for building and construction. *Procedia Manuf.* **2019**, *35*, 641–648. [CrossRef]
5. Nizevičienė, D.; Vaičiukynienė, D.; Michalik, B.; Bonczyk, M.; Vaitkevičius, V.; Jusas, V. The treatment of phosphogypsum with zeolite to use it in binding material. *Constr. Build. Mater.* **2018**, *180*, 134–142. [CrossRef]
6. Alaa, M.R. Phosphogypsum as a construction material. *J. Clean. Prod.* **2017**, *166*, 732–743.
7. Fernando, D.C.H.; Holger, S.; Valdecir, A.Q. Influence of phosphorus from phosphogypsum on the initial hydration of Portland cement in the presence of superplasticizers. *Cem. Concr. Compos.* **2017**, *83*, 384–393.
8. Liu, S.; Ouyang, J.; Ren, J. Mechanism of calcination modification of phosphogypsum and its effect on the hydration properties of phosphogypsum-based supersulfated cement. *Constr. Build. Mater.* **2020**, *243*, 118226. [CrossRef]
9. Yelizaveta, C.; Olena, Y.; Viktoriia, C.; Hynek, R. Phosphogypsum recycling: A review of environmental issues, current trends, and prospects. *Appl. Sci.* **2021**, *11*, 1575. [CrossRef]
10. Shu, J.; Zhao, J.; Li, B.; Luo, D.; Zeng, X.; Chen, M.; Liu, Z. Cooperative removal of Mn^{2+}, $NH^{4+}-N$, $PO_4{}^{3-}-P$ and F^- from electrolytic manganese residue leachate and phosphogypsum leachate. *J. Cent. South Univ.* **2022**, *29*, 3656–3669. [CrossRef]
11. Gu, Q.; Lin, X.; Zhao, S.; Yuan, Y. Effect of different pretreatment processes on properties of phosphogypsum. *Inorg. Chem. Ind* **2022**, *54*, 17–23.
12. Li, X.; Zhang, Q. Dehydration behaviour and impurity change of phosphogypsum during calcination. *Constr. Build. Mater.* **2021**, *311*, 125328. [CrossRef]
13. Zhang, W.; Zhao, L.; Xue, M.; Duan, X.; Feng, C.; Zhu, J. Effect of oxalic acid pretreatment on the mechanical properties and microstructure of phosphogypsum. *Constr. Build. Mater.* **2023**, *362*, 129631. [CrossRef]
14. Cai, Q.; Jiang, J.; Ma, B.; Shao, Z.; Hu, Y.; Qian, B.; Wang, L. Efficient removal of phosphate impurities in waste phosphogypsum for the production of cement. *Sci. Total Environ.* **2021**, *780*, 146600. [CrossRef]
15. Fang, J.; Ge, Y.; Chen, Z.; Xing, B.; Bao, S.; Yong, Q.; Chi, R.; Yang, S.; Ni, B. Flotation purification of waste high-silica phosphogypsum. *J. Environ. Manag.* **2022**, *320*, 115824. [CrossRef]
16. Qi, M.; Peng, W.; Wang, W.; Cao, Y.; Fan, G.; Huang, Y. Simple and efficient method for purification and recovery of gypsum from phosphogypsum: Reverse-direct flotation and mechanism. *J. Mol. Liq.* **2023**, *371*, 121111. [CrossRef]
17. Cao, W.; Yi, W.; Peng, J.; Li, G.; Yin, S. Preparation of anhydrite from phosphogypsum: Influence of phosphorus and fluorine impurities on the performances. *Constr. Build. Mater.* **2022**, *318*, 126021. [CrossRef]
18. Wu, H.; Han, C.; Tang, Y. Research progress on reutilization of phosphogypsum in China. *Mod. Chem. Ind.* **2023**, *43*, 18–21.
19. Wang, J.; Dong, F.; Wang, Z.; Yang, F.; Du, M.; Fu, K.; Wang, Z. A novel method for purification of phosphogypsum. *Physicochem. Probl. Miner. Process.* **2020**, *56*, 975–983. [CrossRef]

20. Du, M.; Wang, J.; Dong, F.; Wang, Z.; Yang, F.; Tan, H.; Fu, K.; Wang, W. The study on the effect of flotation purification on the performance of α-hemihydrate gypsum prepared from phosphogypsum. *Sci. Rep.* **2022**, *12*, 95. [CrossRef] [PubMed]
21. Qiu, Y.; Mao, Z.; Sun, K.; Zhang, L.; Yang, L.; Qian, Y.; Lei, T. Cost-efficient clean flotation of amorphous graphite using water-in-oil kerosene emulsion as a novel collector. *Adv. Powder Technol.* **2022**, *33*, 103770. [CrossRef]
22. Zhang, Y.; Zhu, H.; Zhu, J.; Shi, Q.; Yin, J.; Xu, D.; López, V.A. Characteristic evolution and energy variation during the generation of kerosene droplet. *Fuel* **2021**, *288*, 119684. [CrossRef]
23. Gui, X.; Xing, Y.; Wang, T.; Cao, Y.; Miao, Z.; Xu, M. Intensification mechanism of oxidized coal flotation by using oxygen-containing collector α-furanacrylic acid. *Powder Technol.* **2017**, *305*, 109–116. [CrossRef]
24. Li, L.; Lu, X.; Qiu, J. Effect of microemulsified collector on froth flotation of coal. *J. South. Afr. Inst. Min. Metall.* **2013**, *113*, 877–880.
25. Zhu, X.; He, M.; Zhang, W.; Wei, H.; Lyu, X.; Wang, Q.; You, X.; Li, L. Formulation design of microemulsion collector based on gemini surfactant in coal flotation. *J. Clean. Prod.* **2020**, *257*, 120496. [CrossRef]
26. Wang, M.; Yuan, X.; Dong, W.; Fu, Q.; Ao, X.; Chen, Q. Gradient removal of Si and P impurities from phosphogypsum and preparation of anhydrous calcium sulfate. *J. Environ. Chem. Eng.* **2023**, *11*, 110312. [CrossRef]
27. Qiao, X.; Liu, A.; Li, Z.; Fan, J.; Fan, P.; Fan, M. Preparation and properties of dodecylamine microemulsion for the flotation of quartz and magnetite. *Miner. Eng.* **2021**, *164*, 106821. [CrossRef]
28. Abarca, C.; Ali, M.M.; Pelton, R.H. Choosing mineral flotation collectors from large nanoparticle libraries. *J. Colloid Interface Sci.* **2018**, *516*, 423–430. [CrossRef] [PubMed]
29. McClements, D.J. Nanoemulsions versus microemulsions: Terminology, differences, and similarities. *Soft Matter* **2012**, *8*, 1719–1729. [CrossRef]
30. Zolfaghari, M.; Nasiri, M.; Haghighi Asl, A. Properties and Phase Behavior of Water-Tween-Kerosene Microemulsions and Prediction of Their Viscosity. *Chem. Eng. Technol.* **2023**, *46*, 2081–2089. [CrossRef]
31. Chen, Y.; Xia, W.; Xie, G. Contact angle and induction time of air bubble on flat coal surface of different roughness. *Fuel* **2018**, *222*, 35–41. [CrossRef]
32. Wang, D.; Xu, M.; He, J.; Wang, L. Flotation of low rank coal using dodecane after pretreatment by dielectric barrier discharge (DBD) air plasma. *Fuel* **2019**, *251*, 543–550. [CrossRef]
33. Bera, A.; Kumar, T.; Ojha, K.; Mandal, A. Adsorption of Surfactants on Sand Surface in Enhanced Oil Recovery: Isotherms, Kinetics and Thermodynamic Studies. *Appl. Surf. Sci.* **2013**, *284*, 87–99. [CrossRef]
34. Koneva, A.S.; Safonova, E.A.; Kondrakhina, P.S.; Vovk, M.A.; Lezov, A.A.; Chernyshev, Y.S.; Smirnova, N.A. Effect of Water Content on Structural and Phase Behavior of Water-in-oil (n-decane) Microemulsion System Stabilized by Mixed Nonionic Surfactants SPAN80/TWEEN80. *Colloids Surf. A Physicochem. Eng. Asp.* **2017**, *518*, 273–282. [CrossRef]
35. Al-Dabbas, M.A.; Eisa, M.Y.; Kadhim, W.H. Estimation of gypsum-calcite percentages using a Fourier transform infrared spectrophotometer (FTIR), in Alexandria Gypsiferous Soil-Iraq. *Iraqi J. Sci.* **2014**, *55*, 1916–1926.
36. Luo, B.; Zhu, Y.; Sun, C.; Li, Y.; Han, Y. The flotation behavior and adsorption mechanisms of 2-((2-(decyloxy) ethyl) amino) lauric acid on quartz surface. *Miner. Eng.* **2018**, *117*, 121–126. [CrossRef]
37. Xia, W.; Li, Y.; Nguyen, V.A. Improving coal flotation using the mixture of candle soot and hydrocarbon oil as a novel flotation collector. *J. Clean. Prod.* **2018**, *195*, 1183–1189. [CrossRef]
38. Zeng, H.; Xing, B.; Cao, Y.; Xu, B.; Hou, L.; Guo, H.; Cheng, S.; Huang, G.; Zhang, C.; Sun, Q. Insight into the microstructural evolution of anthracite during carbonization-graphitization process from the perspective of materialization. *Int. J. Min. Sci. Technol.* **2022**, *32*, 1397–1406. [CrossRef]